ACS Sustainable Chemistry & Engineering

Research Article

pubs.acs.org/journal/ascecg

Value-Added Biopolymer Nanocomposites from Waste Eggshell-Based $CaCO_3$ Nanoparticles as Fillers

Tarig A. Hassan, Vijaya K. Rangari,* and Shaik Jeelani

Department of Materials Science and Engineering, Tuskegee University, Tuskegee, Alabama 36088, United States

ABSTRACT: Waste eggshells were used as a raw material to produce high surface area biocalcium carbonate nanoparticles using a combination of mechanochemical and ultrasonic irradiation techniques. High resolution transmission electron microscopy (HR-TEM) and X-ray analysis showed that the synthesis process was effective and yields only $CaCO_3$ nanoparticles with high porosity. The bionanocomposites were prepared by infusing three different weight percentages (1%, 2%, and 3%) of the calcium carbonate nanoparticles ($CaCO_3$) in Bioplast GS 2189 thermoplastic polymer. Thermal analyses indicated that the 2% bionanocomposites are thermally more stable (by 15 °C) than the corresponding neat systems. Mechanical test results of 2% bionanocomposite showed an approximately 35.3% and 30.5% increase in the flexural strength and modulus, respectively, over the pristine Bioplast GS 2189 polymer.

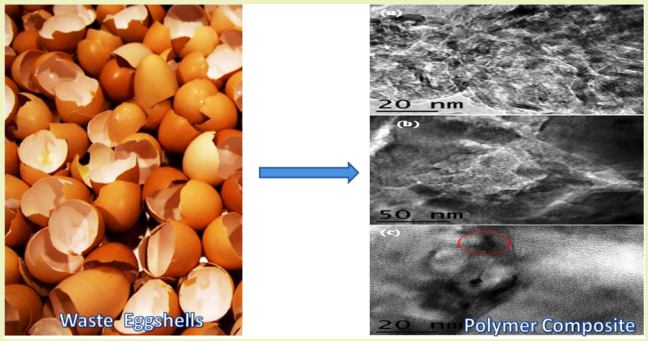

KEYWORDS: *Biodegradable polymers, Renewable materials, Mechanical properties, Calcium carbonate, Nanocomposites*

INTRODUCTION

Sustainable biobased polymer composites have been the subject of intense research in recent years. Currently, there is a serious demand for new green materials and composites in all applications. This growing demand is derived from the implementation of new environmental regulations around the world. Moreover, petroleum-based resources are getting more expensive and are being depleted at a very high rate in addition to their destructive impact on the environment. On the other hand, biobased polymer composites are developed from renewable resources so they are environmentally friendly and do not contribute to the depletion of energy resources, offering great energy and greenhouse gas emission savings.[1,2]

Many natural and biobased materials like soy bean oil have been utilized in the creation of different biopolymers and composites.[3−6] Various biodegradable thermoplastic polymers are developed from plant-based materials such as different types of starches and sugars along with polylactic acid (PLA).[7,8] These materials are employed in a wide range of engineering applications due to their economical and environmental advantages compared to petroleum-based materials and have comparable properties. Biobased polymer nanocomposite materials have been extensively studied due to their remarkable combinations of properties.[9−12] Also, a number of United States patents in biobased polymers have been issued.[13−16]

One of the most important means to alter the mechanical and thermal properties of polymers is through the use of various kinds of soft/hard fillers. Current research efforts focus on the use of filler materials in the nanometer scale to improve different properties of polymers. A major application of nanoparticles is their use as nanofillers to enhance the properties of pristine thermoset and thermoplastic polymeric materials. Finding renewable resources for the development of new environmentally friendly and biobased fillers are also essential and has attracted substantial global interest. Lin and co-workers have reported the preparation of a shell/β-polypropylene biocomposite. Incorporation of the biobased micrometer-sized shell powder derived from fisheries waste have substantially improved the impact strength of the resultant biocomposite by 240% compared to the neat polypropylene.[17]

Eggshell represents a great source of biobased calcium carbonate that can be efficiently used as biofiller in polymer nanocomposites.[18−22] This natural bioceramic composite is abundantly available and has an exceptional chemical composition that consists of high inorganic content (~95% of calcium carbonate) and about 4% organic components.[23−25] The mechanical properties of the eggshells are influenced by the interaction between these organic and inorganic constituents making it suitable for use as fillers.[26,27] Takamine at el. studied the effect of eggshell on the properties of corn starch extrudates. They reported that the addition of up to 10% eggshell has increased the shear strength of extrudates.[28] Xu and Hanna studied the use of micrometer-sized eggshell particles as a nucleating agent in a composite foam material derived from corn starch that was used for food packaging application. The composite foam was prepared by extrusion

Received: October 4, 2013
Revised: January 12, 2014
Published: January 23, 2014

and characterized to investigate the effects of eggshell on the structure, morphology, and physical and mechanical properties, as well as the thermal stability of the foam. The foam properties were significantly enhanced and foam thermal transition and stability increased with the addition of 6% loading of the eggshell.[29] Bootklad and Kaewtatip investigated the use of eggshells as filler in a biodegradable thermoplastic starch composite prepared using compression molding. The effect of incorporation of the micrometer-sized eggshell powder on the properties of thermoplastic starch was compared with the effect of commercial calcium carbonate particles. The eggshell/thermoplastic starch composite achieved better adhesion between the filler powder and the matrix and improved water resistance and thermal stability compared to commercial calcium carbonate/thermoplastic starch composites that were more rapidly degraded.[30]

These studies have described the use of micrometer-sized eggshell particles in polymeric composites as reinforcement fillers at relatively high loadings.[18−21,29,30] The objective of this research is to study the effect of infusion of small amounts (1%, 2%, and 3% by weight) of high surface area nano-sized biocalcium carbonate particles derived from eggshells in biobased biodegradable thermoplastic polymer on the thermal and mechanical properties of the resultant bionanocomposites.

MATERIALS AND METHODS

Materials. In this study, we have used biobased materials that have been acquired from renewable resources. The primary source of our biobased nanofiller is waste eggshells that were obtained from American Dehydrated Foods, Inc. (Social Circle, GA), a local food processing company. These waste eggshells were used as raw material for the synthesis of bio-$CaCO_3$ nanoparticles. Commercially available Bioplast GS 2189 was used as the polymeric matrix. Bioplast GS 2189 is a completely biodegradable thermoplastic polymer in the form of small, white, spherical-like pellets of 3 mm in size and was purchased from Biotec Distribution (The Netherlands). Chloroform was used as a solvent in the solution mixing process, and it was purchased from Sigma-Aldrich (St. Louis, MO).

Processing and Fabrication of Bio-$CaCO_3$/Bioplast GS 2189 Bionanocomposites. Bio-$CaCO_3$ nanoparticles used in this investigation were derived from chicken eggshells. The nanoparticles have been synthesized via a top-down approach for producing nanostructured materials. The first step was cleaning and drying of the eggshells. The shells were then ground with a grinder to produce fine powder that was then subjected to further size reduction via a mechanical attrition method. After that, the particle sizes were standardized by passing through a set of standard stainless steel sieves 95 and 20 μm in size using a Retsch high speed shaker. Further size reduction was carried out using a sonochemical method to produce bio-$CaCO_3$ nanoparticles of size less than or equal to approximately 10 nm with a BET surface area of approximately 44 m^2/g.[27] The sonochemical technique is extensively reported in the literature for size reduction of different bulk materials to nanoscale materials.[31,32] The sonochemical processing is considered to be one of the most efficient techniques for generating novel materials with remarkable properties. Sonochemistry arises from the acoustic cavitation phenomenon, that is, the formation, growth, and implosive collapse of bubbles in a liquid medium.[31] The extremely high temperatures (>5000 K), pressures (>20 MPa), and very high cooling rates ($>10^7$ K s^{-1})[32] attained during cavity collapse lead to many unique properties in the irradiated solution. Using these extreme conditions, researchers have been able to synthesize several materials; this technique has proven to be a unique method for size reduction. Franco et al. stated that sonication is an effective tool for reducing the particle size of different inorganic materials, while the crystalline structure is retained.[33−35] During the sonochemical irradiation phase, three different organic solvents were used. There are a number of parameters affecting the sonochemical technique for synthesis of nanoparticles; one of the important parameters is the liquid vapor pressure.[36] There is a direct effect of the solvent used during sonication and the reaction outcome. Nanostructured materials can be prepared by the sonochemical route in low volatility solvents that have relatively low vapor pressures. Solvents with low vapor pressures are expected to have better sonochemical effects and lead to better reaction results.[36] The sonochemical effect of DMF is more pronounced, and the particles were irregular platelets of ∼10 nm. The BET surface area (43.687 m^2/g) of these nanoparticles is much higher than that of nanoparticles from other solvents such as decaline and THF (R). The excellent sonication effect of DMF was also confirmed by the studies of other researchers.[37,38] During the sonochemical step, eggshell particles were irradiated with a high intensity ultrasonic horn (Ti-horn, 20 kHz, and 100 W/cm^2) in the presence of dimethylformamide (DMF) for 5 h. The synthesis process is described in detail in our previous paper.[39]

The as-prepared bio-$CaCO_3$ nanoparticles were used as reinforcing filler in Bioplast GS 2189 thermoplastic polymer. Bio-$CaCO_3$/Bioplast GS 2189 nanocomposites were fabricated using a Wayne Yellow Label table top single screw melt extruder. One of the big challenges in the fabrication of bio-$CaCO_3$/Bioplast GS 2189 nanocomposites was the initial mixing of the bio-$CaCO_3$ nanoparticles and the 3 mm polymer pellets. To incorporate the nanofiller in the polymer matrix and achieve a good dispersion of the bio-$CaCO_3$ nanoparticles in the Bioplast GS 2189 polymer, a solution mixing process was used. In this process, Bioplast GS2189 polymer was completely dissolved in chloroform, and the bio-$CaCO_3$ nanoparticles were further dispersed in the polymer/chloroform solution by ultrasonic irradiation. Chloroform was used as a solvent because of high polymer solubility at room temperature. In addition, it can be easily removed from the polymer/nanoparticles mixture after the process. In a typical experiment, 100 g of Bioplast GS 2189 polymer pellets were dissolved in 600 g of chloroform in a glass beaker, and known weight percentages bio-$CaCO_3$ nanoparticles were added to the polymer/chloroform solution. Three different weight percentages of the bio-$CaCO_3$ nanoparticles were used (1%, 2%, and 3%). The mixture of polymer/chloroform solution and bio-$CaCO_3$ nanoparticles was stirred for 24 h using a magnetic stirrer to ensure that the polymer has completely dissolved into the chloroform; when the bio-$CaCO_3$ nanoparticles are infused in the mixture, an absolutely homogeneous solution will result. In the next step, the polymer/chloroform solution containing the bio-$CaCO_3$ nanoparticles was irradiated with high intensity ultrasonic horn (Ti-horn, 20 kHz, 100 W/cm^2) at 50% amplitude for 30 min at room temperature. The sonochemical technique is efficient in producing high quality monodispersed nanocomposites.[40] To control the process temperature and avoid heating of the contents and solvent evaporation, the beaker was immersed in a coolant, and the coolant temperature was controlled by a thermostatted bath at 5 °C. After the ultrasonic irradiation step, the polymer/bio-$CaCO_3$ nanoparticles composite mixture was precipitated by addition of excess amounts of methyl alcohol. This uniform mixture of Bioplast GS 2189 polymer and bio-$CaCO_3$ nanoparticles was then collected in the form of powder and dried under vacuum in a conventional oven at 65 °C for 48 h to ensure complete removal of the solvent and methanol residues from the composite mixture. The solution mixing method was followed for the preparation and dispersion of all weight fractions of the nanoparticles in the Bioplast GS 2189 polymer including 1%, 2%, and 3% loadings. Neat polymer pellets were also converted into polymer powder using the same procedure for comparison.

The Bioplast GS 2189 polymer and bio-$CaCO_3$ nanoparticles powder mixture was then extruded using a Wayne Yellow Label table top single screw extruder. The extruder has a 19 mm diameter screw, which is driven by a 2 HP motor via a toothed timing belt for smooth speed variations. Thermostatically controlled five heating zones were used to melt the mixture prior to extrusion, three of which were occupied by the barrel zone and the other two by the die zone. The heaters inside the barrel zone were set at temperatures above the melting temperature of the Bioplast GS 2189 polymer. Table 1 shows the temperatures of the heating zones of the extruder along with die zones 1 and 2.

Table 1. Temperature Settings of the Extrusion Process

temperature (°C)				
zone 1	zone 2	zone 3	die zone 1	die zone 2
148.9	151.7	154.4	160.0	162.2

The purpose of these three heating zones is to maintain a gradually increasing temperature in the molten polymer. The process began by pouring the polymer/nanoparticles mixed powder through the feed hopper. As the mixture reached the barrel zone, the polymer started melting due to high barrel temperature. The outer surface of the extruder screw is designed to maintain a close fit with the barrel's inner surface. As a result, the molten mass cannot escape from the screw surface. As the extruder screw rotates, the molten matrix was further mixed with the bio-$CaCO_3$ nanoparticles, conveyed in a spiral pattern, and then reached the screw end, which is located right before the die zone. The screw end is shaped in a way that allows the flowing mass to escape through a narrow opening at high velocity. The die zone consists of two parts; one is the die itself and the other part is a rectangular stainless steel sample mold. The stainless steel sample mold was attached to the extruder and has the shape and dimensions of a flexural sample so that the extruded nanocomposite samples take the shape of a flexure test specimen according to ASTM D790-02. The stainless steel sample mold is composed of two stainless steel parts that attached to each other by 10 screws with a sample mold trapped in between. Before the mold was attached to the extruder, it was cleaned, sprayed with freekote (releasing agent for easy removal of the sample after the process), then assembled, and attached to the extruder die end. Eight steel bars were inserted into four holes in each stainless steel part to heat up the mold. A thermocouple was attached to the bottom of the lower part of the mold to measure the mold temperature (die zone 2). The mold is equipped with a circular cooling system. The two heaters in the die zone were set at a temperature of 162.2 °C to maintain constant temperature of the flowing mass. One of the heaters was placed after the circular plate, and the other one was the steel bars inserted into the sample mold. As the bulk materials passed through the plate, they were diverted into several branches and then combined again. This ensured a distributive mixing of the nanofillers with polymer.[41] The polymer melt and bionanoparticles mixture passed through the 100 mm long steel tube and approached the die area. As the liquid Bioplast GS 2189 polymer containing the bio-$CaCO_3$ nanoparticles arrived at the die area, the molten masses were extruded and pushed into the sample mold. The extruded sample filled the mold, and the excess amount of the sample was dispensed out of the sample mold through two small holes in the bottom of the mold. Subsequently, the screw and die zone heaters were turned off, and the water cooling system was turned on for 15 min to cool the sample mold to room temperature. The sample was left in the mold for 12 h to completely solidify and was then removed and used for later characterizations. The extrusion process was conducted for neat Bioplast GS 2189 polymer as well as for all bio-$CaCO_3$/Bioplast GS 2189 nanocomposites.

Characterization. X-ray diffraction measurements were conducted using a Rigaku D/MAX 2200 X-ray diffractometer to investigate the structure of bio-$CaCO_3$ nanoparticles. XRD measurements were also used to study the exfoliation of bio-$CaCO_3$ in as-prepared bionanocomposites. The XRD samples were prepared by uniformly spreading the bio-$CaCO_3$ nanoparticles on a quartz sample holder, whereas the as-prepared neat polymers and bionanocomposites cured samples were cut precisely into small specimens and mounted in an aluminum sample holder for measurement. XRD tests were conducted at room temperature from 10° to 80° of 2θ. The pattern peaks resulting from the diffraction were analyzed using Jade 9 software.

High-resolution transmission electron microscopy (HR-TEM) has been performed on as-prepared bio-$CaCO_3$ nanoparticles and the 2 wt % bio-$CaCO_3$ nanoparticles-infused Bioplast GS 2189 polymer, using a JEOL-2010 transmission electron microscope. TEM samples were prepared by dispersion of nanoparticles in ethanol using a sonication bath for 5 min at room temperature, and a drop of solution was placed on a copper grid (carbon-coated copper grid, 200 mesh), then dried in air, and used for TEM analysis. The 2% bio-$CaCO_3$ nanoparticles-infused Bioplast GS 2189 bionanocomposites samples were sliced to approximately 100 nm using a diamond blade attached to a Leica EM UC6 microtome.

To study the thermal stability of the neat Bioplast GS 2189 polymer and bio-$CaCO_3$/Bioplast GS 2189 nanocomposite systems prepared in this investigation, thermogravimetric analysis (TGA) of all samples was carried out under a nitrogen gas atmosphere on a Mettler Toledo TGA/SDTA 851e apparatus. The samples were precisely cut into small pieces (~10−20 mg) and kept in an aluminum oxide sample pan. TGA measurements were carried out from 30 to 800 °C at a heating rate of 10 °C/min. Real time characteristic curves were generated by a Mettler data acquisition system. These analyses were carried out according to ASTM Standard E1131-03. DSC experiments were also carried out using a Mettler Toledo DSC 822e. DSC experiments were conducted from room temperature to 500 °C at a heating rate of 10 °C/min under a nitrogen gas atmosphere. The samples were precisely cut into small pieces of 10−20 mg, kept in an aluminum sample pan, and used for DSC analysis. These tests were carried out using ASTM Standard E1356-03.

Dynamic mechanical analysis (DMA) of various specimens was carried out on a TA Instruments dynamic mechanical analyzer DMA Q800. The samples were cut into small pieces using a diamond cutter and machined using a mechanical grinder to maintain the specified sample dimensions. The width of the samples was 12 mm, and the span length to thickness ratio was 10. The test was carried out according to ASTM D4065-01. DMA tests were run on a double cantilever beam mode with a frequency of 1 Hz and amplitude of 15 μm. The temperature was ramped from room temperature to 180 °C, and the heating rate was maintained at 5 °C/min throughout the test runs so that there was a minimum temperature lag between the sample and the furnace environment. From the test data, storage modulus, loss modulus, and tan δ were determined.

Thermo-mechanical analysis (TMA) experiments of the neat Bioplast GS 2189 polymer and bio-$CaCO_3$ reinforced Bioplast GS 2189 polymer nanocomposites were carried out on a TA Instruments thermomechanical analyzer TMA Q400. The samples were cut into small pieces of dimensions 5 mm × 5 mm × 5 mm using a diamond cutter and machined using a mechanical grinder to maintain the specified sample dimensions according to standard ASTM E 831-06. Dimensional changes were measured in the thickness direction, and the temperature was ramped from room temperature to 180 °C.

Flexural tests under a three-point bend (TPB) configuration were performed according to ASTM D790-02. Test specimens length and width are 100 and 13 mm, respectively. The span length is 80 mm, and average sample thickness is 4.8 mm. The tests were conducted in a 2.5 kN Zwick Roell Z 2.5 testing machine equipped with TestXpert data-acquisition system. The machine was operated under displacement control mode at a crosshead speed of 2.0 mm/min, and all the tests were performed at room temperature. Stress−strain data for each sample was collected. Flexural strength and modulus were calculated from the slope of the stress−strain plot. Five samples were tested from each material, and the average values of flexural strength and modulus were determined. Scanning electron microscopy (SEM) analysis was carried out using a JEOL JSM 5800 scanning electron microscope to study the fracture surface of samples in response to flexural load at the microscopic level. The failed samples of the neat Bioplast GS 2189 polymer and bio-$CaCO_3$/Bioplast GS 2189 nanocomposites were cut into small pieces and placed on a double-sided adhesive conductive carbon tape and coated with a thin layer of a gold/palladium mixture (Au/Pd) using a sputter coater Hummer 6.2 to prevent charge buildup by the electron absorbed by the specimen.

RESULTS AND DISCUSSION

XRD analysis was carried out to investigate the crystal structure of the bio-$CaCO_3$ nanoparticles derived from eggshells. The XRD pattern of bio-$CaCO_3$ nanoparticles is presented in Figure 1a.

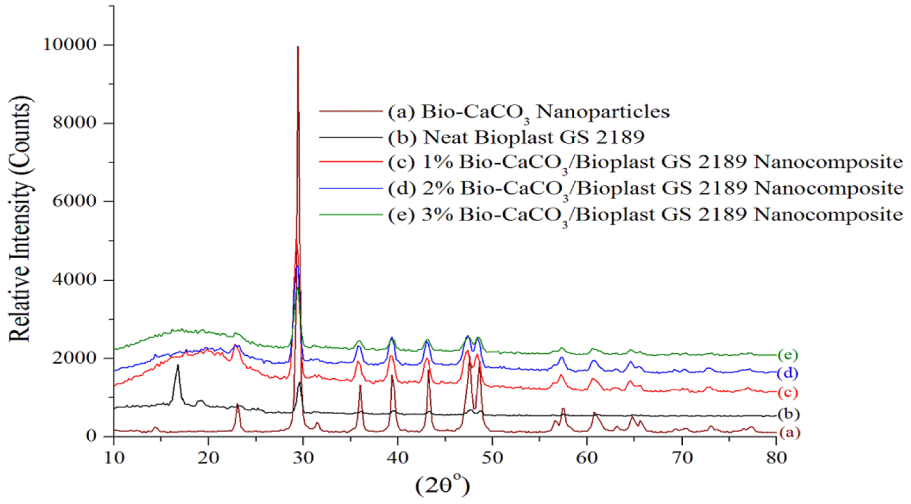

Figure 1. XRD pattern of bio-$CaCO_3$/Bioplast GS 2189 nanocomposites.

It is observed from the pattern that all the peaks matched very well with calcium carbonate $CaCO_3$ JCPDS card No. 47-1743 of calcite. Also, the pattern does not show any peaks of impurities in the sample, which clearly suggests the high purity of inorganic calcium carbonate in the bioinspired nanoparticles. The XRD pattern of the neat Bioplast GS 2189 polymer is presented in Figure 1b and shows crystalline peaks at 17°, 19°, and 30° of 2θ. These results are consistent with the polymer data sheet.

The characteristic peaks in XRD patterns of Figure 1(a−e) also match with the $CaCO_3$ JCPDS card No. 47-1743. An additional wide peak at approximately 18° of 2θ is noticeable in all bio-$CaCO_3$/Bioplast GS2189 nanocomposites. This distinct wide peak corresponds to the polymer. XRD data show a significant decrease in the intensities of the characteristic $CaCO_3$ peaks between the XRD pattern of pure bio-$CaCO_3$ nanoparticles and the XRD patterns for the as-prepared Bioplast GS 2189 polymer nanocomposites. Reduction in the peak intensities indicate that the bio-$CaCO_3$ nanoparticles are highly exfoliated in the polymer matrix, and this may be the result of good dispersion of the bio-$CaCO_3$ nanoparticles in Bioplast GS 2189 polymer.[40] Good dispersion was achieved by the efficient solution mixing procedure and proper extrusion temperatures used in the fabrication process.

TEM was used to determine the characteristics of as-prepared bio-$CaCO_3$ nanoparticles. A TEM micrograph of bio-$CaCO_3$ nanoparticles is presented in Figure 2a. TEM results show that all bio-$CaCO_3$ nanoparticles are uniform in particle sizes less than 10 nm. The TEM image also indicates that the bio-$CaCO_3$ nanoparticles demonstrate highly crystalline structures along with irregular shapes that justify the high surface area of these nanoparticles.

Transmission electron microscopy was also used to investigate the dispersion of bio-$CaCO_3$ nanoparticles in the Bioplast GS 2189 polymer, and the results showed that the as-prepared bio-$CaCO_3$ nanoparticles are superbly dispersed in the polymer matrix. Figures 2b and c show TEM micrographs of the 2% bio-$CaCO_3$/Bioplast GS 2189 nanocomposite. The TEM micrograph in Figure 2b indicates good dispersion of the bionanoparticles over the entire volume of the polymer, and Figure 2c displays a very good dispersion also and clearly shows that there is no agglomeration of bio-$CaCO_3$ nanoparticles in the polymer with a relatively high number of particles in a given small volume of polymer even at a relatively high magnification. Furthermore, these TEM results illustrate the highly crystalline

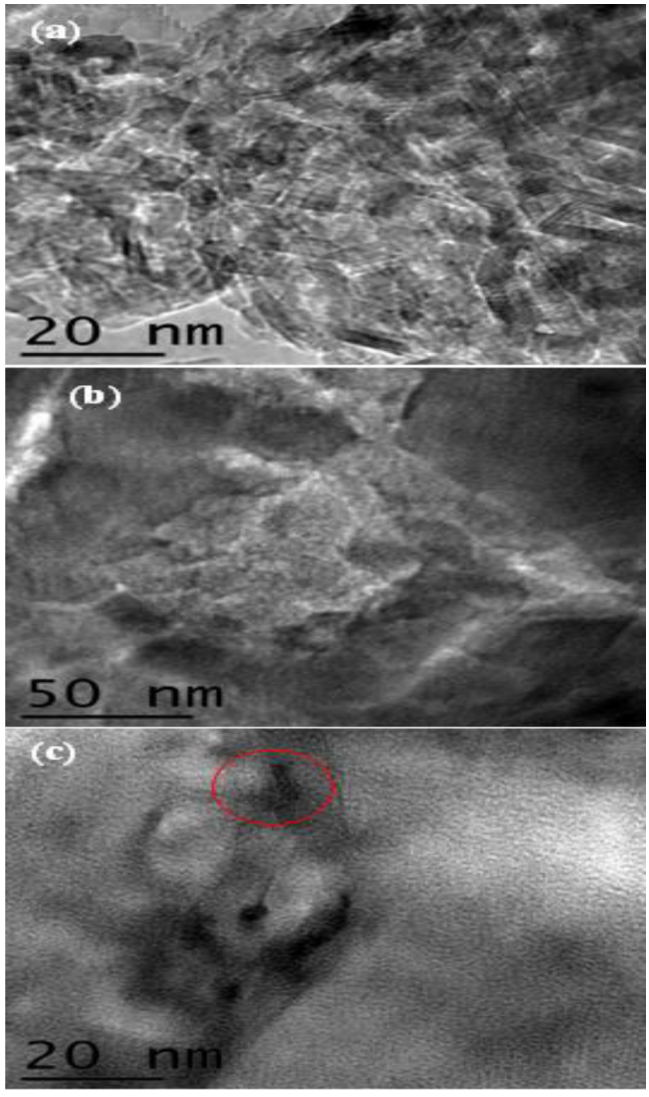

Figure 2. TEM micrographs of (a) bio-$CaCO_3$ nanoparticles and (b, c) 2% bio-$CaCO_3$/Bioplast GS 2189 nanocomposite.

dx.doi.org/10.1021/sc400405v | ACS Sustainable Chem. Eng. 2014, 2, 706−717

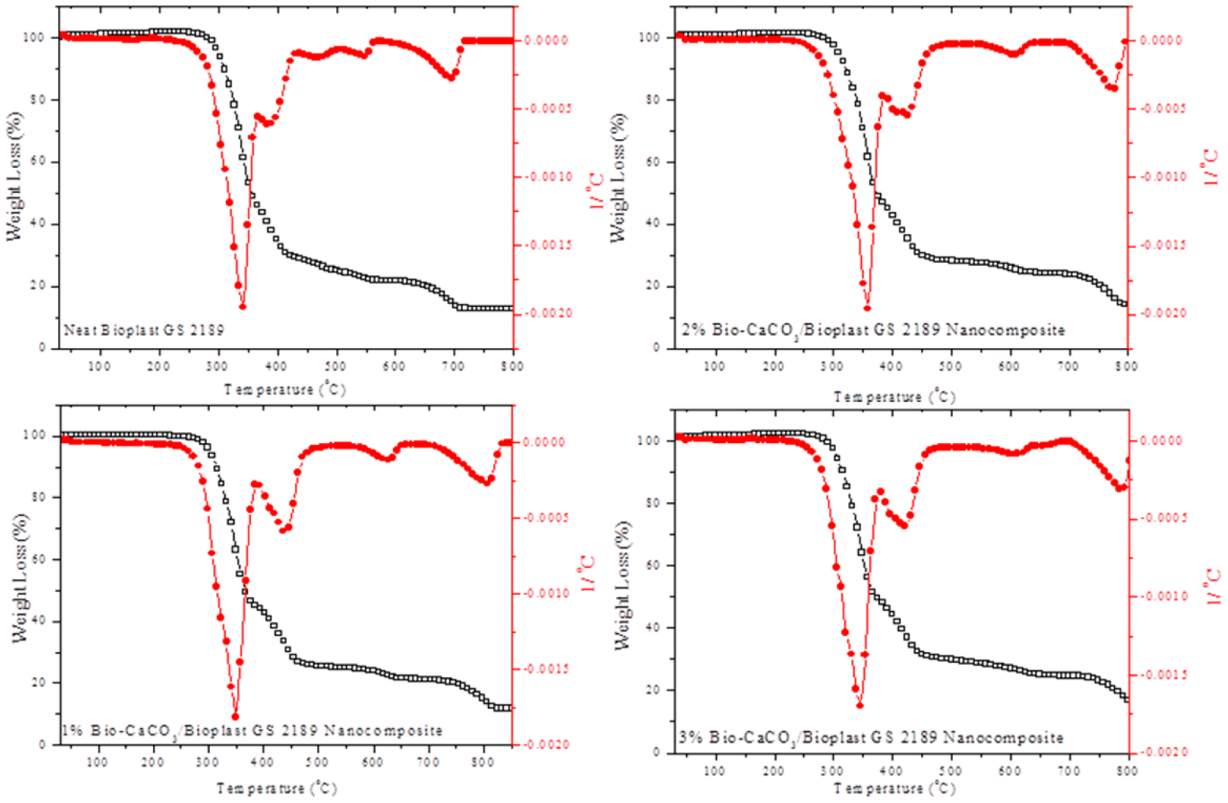

Figure 3. TGA results for neat Bioplast GS 2189 and bio-$CaCO_3$/Bioplast GS 2189 nanocomposites.

Table 2. TGA Results for Neat Bioplast GS 2189 Polymer and Bio-$CaCO_3$/Bioplast GS 2189 Nanocomposites

no.	sample	decomposition temperature T_d (°C)	degrees increased	50% weight loss temperature (°C)	degrees increased
1	neat Bioplast GS 2189	342.2 ± 1.1	–	361.4 ± 2.2	–
2	1% bio-$CaCO_3$/Bioplast GS 2189 nanocomposite	349.0 ± 1.7	06.8	367.2 ± 1.6	05.8
3	2% bio-$CaCO_3$/Bioplast GS 2189 nanocomposite	357.8 ± 2.1	15.6	371.7 ± 1.4	10.3
4	3% bio-$CaCO_3$/Bioplast GS 2189 nanocomposite	345.3 ± 0.9	03.1	369.5 ± 1.2	08.1

nature of the bio-$CaCO_3$ nanoparticles with very distinguished lattice planes presented in the TEM micrographs.

The thermal stability of the as-fabricated neat Bioplast GS 2189 polymer and bio-$CaCO_3$/Bioplast GS 2189 nanocomposites were characterized by TGA. In the present TGA studies, the peak of the derivative curve was considered as a marker for structural decomposition of the samples.[42,43] Figure 3 shows the TGA graphs for the neat Bioplast GS 2189 polymer and bio-$CaCO_3$/Bioplast GS 2189 nanocomposites. As shown in Figure 3a, the decomposition temperature of neat Bioplast GS 2189 is measured at 342 °C. This temperature is assigned to the decomposition of polylactic acid (PLA) in the Bioplast GS 2189 polymer, while it is measured at 349 °C for bio-$CaCO_3$/Bioplast GS 2189 nanocomposites loaded with 1 wt % of the nanofiller as shown in Figure 3b.[44] The highest decomposition temperatures among all tested samples was measured at 358 °C for 2 wt % of bio-$CaCO_3$/Bioplast GS 2189 as presented in Figure 3c. Figure 3d shows the decomposition temperature of the 3% bio-$CaCO_3$/Bioplast GS 2189 nanocomposite at 345 °C. These results clearly show there is a significant increase in the decomposition temperatures of nanophased Bioplast GS 2189 due to the infusion of as-prepared bio-$CaCO_3$ nanoparticles compared to the neat polymer. The improved thermal stability of the bionanocomposite is attributed to the strong adhesion between bio-$CaCO_3$ nanoparticles and the thermoplastic polymer, which stabilizes the bionanocomposite against thermal decomposition.[45] The decomposition temperatures for the neat Bioplast GS 2189 polymer and bio-$CaCO_3$/Bioplast GS 2189 nanocomposites are presented in Table 2 along with the 50% weight loss temperature. From these TGA data, it is evident that the 50% weight loss temperatures of bio-$CaCO_3$/Bioplast GS 2189 nanocomposites have been enhanced considerably over the 50% weight loss temperature of the neat Bioplast GS 2189 polymer. When compared to the 50% weight loss temperature of the neat Bioplast GS 2189 polymer measured from Figure 3(a) at 361 °C, the 50% weight loss temperatures have been increased by 5.8, 10.3, and 8.1 °C for 1%, 2%, and 3% bio-$CaCO_3$/Bioplast GS 2189 nanocomposite, respectively.

TGA graphs also show that all tested samples have experienced three separate weight loss events at higher temperatures. These weight loss events may correspond to the decomposition of certain additives and plasticizers in the commercial Bioplast GS 2189 polymer. It is very much evident from the TGA graphs that all these weight losses temperatures have been shifted toward higher temperatures by several degrees. This also confirms that bio-$CaCO_3$/Bioplast GS 2189 nanocomposites are thermally more stable as compared to the neat Bioplast GS 2189 polymer because of the presence of bio-$CaCO_3$ nanoparticles.

dx.doi.org/10.1021/sc400405v | ACS Sustainable Chem. Eng. 2014, 2, 706−717

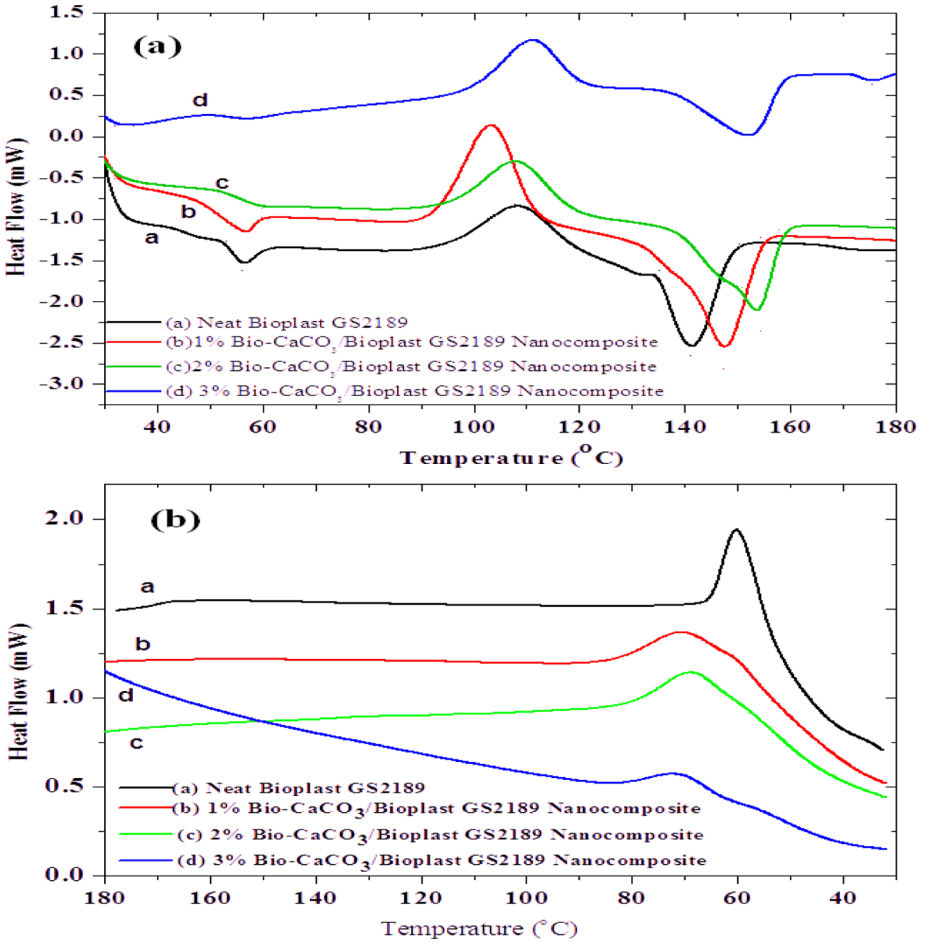

Figure 4. DSC results for neat Bioplast GS 2189 and bio-$CaCO_3$/Bioplast GS 2189 nanocomposites: (a) heating curves, (b) cooling curves.

Table 3. DSC Results for Neat Bioplast GS 2189 and Bio-$CaCO_3$/Bioplast GS 2189 Nanocomposites

no.	sample	glass transition temperature T_g (°C)	degrees increased	melting temperature T_m (°C)	degrees increased	crystallization temperature T_c (°C)	degrees increased
1	neat Bioplast GS 2189	56.2 ± 1.2	–	141.1 ± 0.9	–	60.0 ± 1.0	–
2	1% bio-$CaCO_3$\Bioplast GS 2189 nanocomposite	57.4 ± 0.8	1.2	147.2 ± 1.2	06.1	70.6 ± 0.7	10.6
3	2% bio-$CaCO_3$\Bioplast GS 2189 nanocomposite	60.2 ± 1.0	4.0	154.0 ± 1.1	12.9	67.8 ± 1.3	07.8
4	3% bio-$CaCO_3$\Bioplast GS 2189 nanocomposite	56.4 ± 0.7	0.2	151.0 ± 1.8	02.9	73.76 ± 1.1	13.8

DSC experiments were carried out to estimate the glass transition temperature (T_g), melting temperature (T_m), and crystallization temperature of neat Bioplast GS 2189 and bio-$CaCO_3$/Bioplast GS 2189 nanocomposites. The DSC results are shown in Figure 4a for the heating cycle and Figure 4b for the cooling cycle, and the results are summarized in Table 3. As shown in Figure 4a, all tested samples experience three distinctive thermal events. All samples show glass transition as a wide baseline shift at temperatures in the range of 50−60 °C. Neat Bioplast GS 2189 shows T_g at approximately 56 °C, while 1% bio-$CaCO_3$/Bioplast GS 2189 show glass transition at approximately 58 °C. The T_g values for 2% and 3% bio-$CaCO_3$/Bioplast GS 2189 nanocomposites are obtained at ∼60 °C and ∼56 °C, respectively. It is clear that all bio-$CaCO_3$/Bioplast GS 2189 nanocomposites have increased the glass transition temperatures due to the incorporation of the bio-$CaCO_3$ nanoparticles.

Interestingly, each sample exhibits an exothermic peak at a temperature range of 100−110 °C. These exothermic peaks are noticed prior to samples melting, and they correspond to cold crystallization of the samples due to the reorganization of amorphous into crystalline domains on account of the increased macromolecular flexibility and mobility upon increasing temperature.[46] The samples then approach the melting region, which is represented as a wide endothermic peak at 140−155 °C. The melting point of neat Bioplast GS 2189 polymer is at 141.1 °C. Bio-$CaCO_3$/Bioplast GS 2189 nanocomposites showed a significant increase in the melting temperature by 6.1 °C for 1% bio-$CaCO_3$/Bioplast GS 2189 (147.2 °C), by 12.9 °C for 2% bio-$CaCO_3$/Bioplast GS 2189 (154 °C), and by 2.9 °C for 3% bio-$CaCO_3$/Bioplast GS 2189 (151 °C). As observed from Figure 4a, all bionanocomposite samples showed higher heat of fusion compared to the neat Bioplast polymer, which also indicates better interfacial properties between bio-$CaCO_3$ nanoparticles and the polymer.

dx.doi.org/10.1021/sc400405v | ACS Sustainable Chem. Eng. 2014, 2, 706−717

In the cooling curves presented in Figure 4b, it is observed that all loadings of bio-$CaCO_3$ nanoparticles caused an increase in the crystallization temperature (T_c) compared to the neat Bioplast GS 2189. The crystallization temperature for the neat Bioplast GS 2189 is approximately 60 °C, and it is approximately 70, 67, and 74 °C for 1%, 2%, and 3% bio-$CaCO_3$/Bioplast GS 2189 nanocomposites, respectively. The increase in the crystallization temperature of the nanophased polymer nanocomposite systems is attributed to the infusion of the bio-$CaCO_3$ nanoparticles. These nanofillers act as nucleating agents in the polymer melts; hence, when the polymers melt and recrystallize, faster nucleation takes place at the site where these nucleating agents are more available, causing a higher crystallization than that of the neat Bioplast GS 2189 polymer. This effect is more significant in the case of the 3% of bio-$CaCO_3$/Bioplast GS 2189 composite, which resulted in a too oblique cooling curve than the pristine polymer.

Furthermore, the presence of the bio-$CaCO_3$ nanoparticles cause crystallization to start earlier and at higher temperatures. As shown in the DSC curves, the broader exothermic peaks of the bio-$CaCO_3$/Bioplast GS 2189 nanocomposites compared to the sharp exothermic peak of the neat Bioplast GS 2189 polymer indicate that crystallization of the bionanocomposites is slower than the crystallization of the pristine polymer. The combination of a larger number of nucleation sites and limited crystal growth produces crystals that have fine grain sizes, which will lead to a material with enhanced thermal and mechanical properties. Similar results were also observed by other researchers.[46,47]

The dynamic mechanical analysis (DMA) reveals information about the amount of energy stored in the nanocomposites as elastic energy and the amount of energy dissipated during mechanical strain, which strongly depends on the geometrical characteristic and the level of dispersion of the reinforcing fillers in the matrix. It also depends on the degree of interaction between the matrix and filler surface.[48] DMA was performed to study how the properties of the neat Bioplast GS 2189 polymer and bio-$CaCO_3$/Bioplast GS 2189 nanocomposites are affected by the increase in temperature. Storage modulus, loss modulus, and phase lag (tan δ) for neat and nanophased polymers were measured. The values of storage modulus (E′) for the neat Bioplast GS 2189 polymer and bio-$CaCO_3$/Bioplast GS 2189 nanocomposites with different weight fractions are presented in Figure 5, and the results are compared in Table 4 for three different temperatures. It is shown in Figure 5 that the neat Bioplast GS 2189 polymer has a much lower storage modulus (796.9 MPa) than the bio-$CaCO_3$/Bioplast GS 2189 samples (941.6, 968.2, and 892.6 MPa for 1%, 2%, and 3% bio-$CaCO_3$/Bioplast GS 2189 nanocomposite, respectively) at room temperature. When the temperature was increased to 60 °C, the storage modulus for all samples decreased. The Bioplast GS 2189 nanocomposite sample with 2% bio-$CaCO_3$ nanoparticles loading has the highest storage modulus value at this temperature (800.1 MPa) compared to neat Bioplast GS 2189 (679.9 MPa), 1% bio-$CaCO_3$/Bioplast GS 2189 (743.1 MPa), and 3% bio-$CaCO_3$/Bioplast GS 2189 (713.9 MPa). At higher temperature (100 °C), all the samples passed the softening stage, and the storage modulus values dropped as listed in Table 4. The improvement in the storage modulus of bionanocomposites is due to the presence of highly exfoliated bio-$CaCO_3$ nanoparticles in the polymer matrix. Figure 5 shows the variation of the loss modulus of the neat Bioplast GS 2189 and bio-$CaCO_3$/Bioplast GS 2189 nanocomposites with

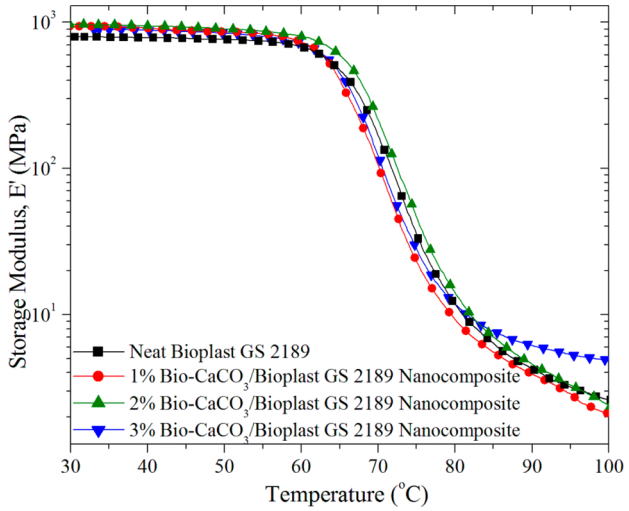

Figure 5. Storage modulus for neat Bioplast GS 2189 and bio-$CaCO_3$/Bioplast GS 2189 nanocomposites.

temperature, and the results are shown in Table 5. As shown in Figure 5, all the curves show a characteristic peak between temperatures of 65−70 °C; these peaks correspond to the glass transition. The glass transition temperatures (T_g) are usually interpreted as the peak of either the tan δ or the loss modulus curves obtained during the dynamic mechanical test; in this study, the peaks of tan δ curves were used to determine the glass transition temperatures (T_g) of the neat Bioplast GS 2189 and bio-$CaCO_3$/Bioplast GS 2189 nanocomposites.[49]

As shown in Figure 6, there is an improvement in the loss modulus of the 1% bio-$CaCO_3$/Bioplast GS 2189 nanocomposite at 30 °C (47 MPa) compared to neat Bioplast GS 2189 polymer (32.7 MPa), 2% bio-$CaCO_3$/Bioplast GS 2189 nanocomposite (28.6 MPa), and 1% bio-$CaCO_3$/Bioplast GS 2189 nanocomposite at 30 °C (34.1 MPa). At 60 °C, the loss modulus has improved for all bio-$CaCO_3$/Bioplast GS 2189 nanocomposites compared to the neat polymer, and as the temperature increased past the softening temperature, loss modulus has diminished for all samples. Moreover, it is noticeable from Figure 6 that the loss modulus peak values increase as an effect of the addition of bio-$CaCO_3$ nanoparticles in Bioplast GS 2189 polymer. The reason for this might be the limitation in the molecular mobility induced by the bionanoparticles.

Figure 7 shows the variation of tan δ with temperature for neat Bioplast GS 2189 and bio-$CaCO_3$/Bioplast GS 2189 nanocomposites. As shown in the figure, all the curves are closely packed and overlaid; however, several observations are noticed. The peak heights of tan δ curves for the bio-$CaCO_3$/Bioplast GS 2189 nanocomposites have been reduced with the introduction of bio-$CaCO_3$ nanoparticles compared to the height of the neat Bioplast GS 2189 polymer curve. All peaks are lowered with the increase in the loading of bio-$CaCO_3$ nanoparticles. The reason may be due to the restriction of the mobility of the polymer chains by the bio-$CaCO_3$ nanoparticles. The other prominent effect is a broadening of the transition region. This may be due to the inhibition of the relaxation process within the bionanocomposites upon incorporation of the bio-$CaCO_3$ nanoparticles.[50] Glass transition temperatures obtained from the peaks of tan δ curves are presented in Table 6. The bio-$CaCO_3$/Bioplast GS 2189 nanocomposite with 2% loading of the particles have the highest T_g (76.1 °C) compared

Table 4. Storage Modulus for Neat Bioplast GS 2189 and Bio-$CaCO_3$/Bioplast GS 2189 Nanocomposites

		storage modulus (MPa)		
no.	sample	at 30 °C	at 60 °C	at 100 °C
1	neat Bioplast GS 2189	796.9 ± 11.2	679.9 ± 10.0	2.6 ± 0.4
2	1% bio-$CaCO_3$/Bioplast GS 2189 nanocomposite	941.6 ± 13.4	743.1 ± 14.5	2.0 ± 0.1
3	2% bio-$CaCO_3$/Bioplast GS 2189 nanocomposite	968.2 ± 09.6	800.1 ± 11.7	2.3 ± 0.3
4	3% bio-$CaCO_3$/Bioplast GS 2189 nanocomposite	892.6 ± 12.1	713.9 ± 12.9	4.9 ± 1.7

Table 5. Loss Modulus for Neat Bioplast GS 2189 and Bio-$CaCO_3$/Bioplast GS 2189 Nanocomposites

		loss modulus (MPa)		
no.	sample	at 30 °C	at 60 °C	at 100 °C
1	neat Bioplast GS 2189	32.7 ± 3.1	103.2 ± 4.8	0.96 ± 0.2
2	1% bio-$CaCO_3$/Bioplast GS 2189 nanocomposite	47.0 ± 3.2	140.6 ± 3.4	1.17 ± 0.1
3	2% bio-$CaCO_3$/Bioplast GS 2189 nanocomposite	28.6 ± 1.5	138.5 ± 2.7	1.22 ± 0.1
4	3% bio-$CaCO_3$/Bioplast GS 2189 nanocomposite	34.1 ± 1.1	118.2 ± 2.5	1.35 ± 0.1

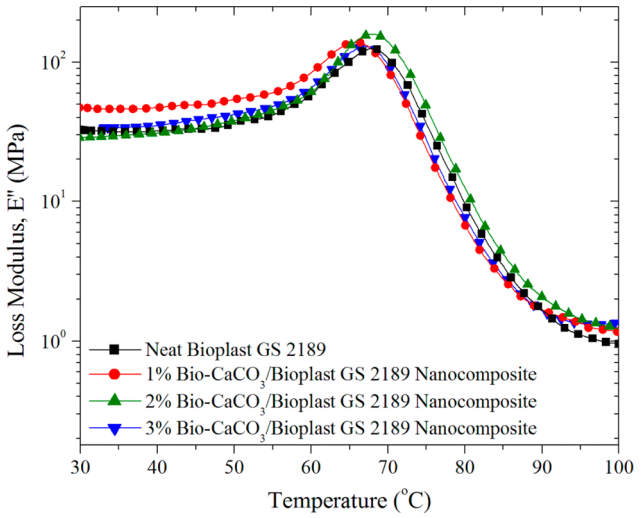

Figure 6. Loss modulus for neat Bioplast GS 2189 and bio-$CaCO_3$/Bioplast GS 2189 nanocomposite.

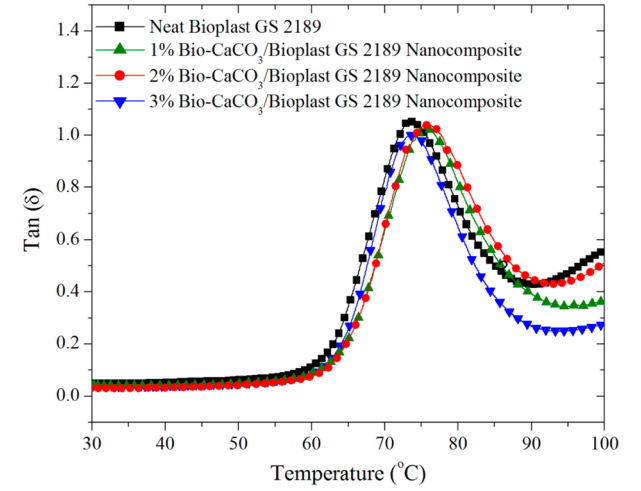

Figure 7. Tan (δ) for neat Bioplast GS 2189 and bio-$CaCO_3$/Bioplast GS 2189 nanocomposites.

to neat Bioplast GS 2189 and the 1% and 3% bio-$CaCO_3$/Bioplast GS 2189 nanocomposites (72.9,, 75.6, and 73.7 °C, respectively). The shifting of T_g to higher temperatures can be associated with the decreased mobility of the matrix chains due

Table 6. Glass Transition Temperatures for Neat Bioplast GS 2189 and Bio-$CaCO_3$/Bioplast GS 2189 nanocomposites measured by DMA

no.	sample	T_g°C
1	neat Bioplast GS 2189	72.9 ± 1.5
2	1% bio-$CaCO_3$/Bioplast GS 2189 nanocomposite	75.6 ± 0.9
3	2% bio-$CaCO_3$/Bioplast GS 2189 nanocomposite	76.1 ± 1.2
4	3% bio-$CaCO_3$/Bioplast GS 2189 nanocomposite	73.7 ± 2.1

to the addition of bio-$CaCO_3$ nanoparticles. These results show that the bio-$CaCO_3$/Bioplast GS 2189 nanocomposite are more thermally stable compared to the neat Bioplast GS 2189 polymer, and they are inconsistent with the TGA and DSC results.

Thermomechanical analysis (TMA) measurements were carried out to obtain information on the dimensional stability of as-prepared bionanocomposites under variation of temperature. The TMA curves for neat Bioplast GS 2189 and bio-$CaCO_3$/Bioplast GS 2189 nanocomposites are presented in Figure 8.

As shown in Figure 8, tested samples show a rather uniform expansion to about 55 °C. Above this temperature, the samples experience a huge extension that takes place due to plastic flow and softening of the polymer, which is followed by melting of the samples at higher temperatures. Bio-$CaCO_3$/Bioplast GS

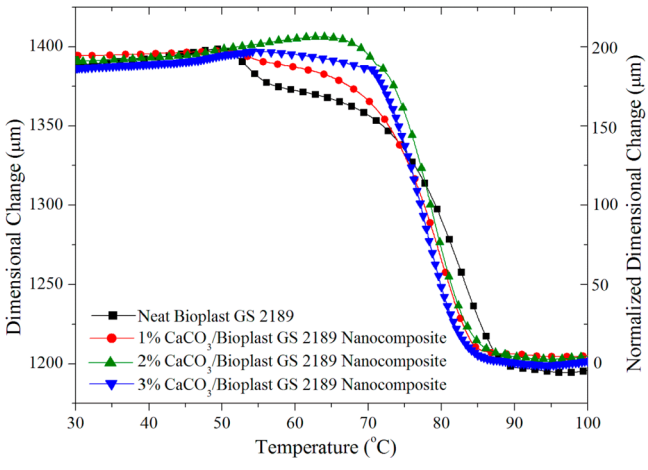

Figure 8. Dimensional change vs temperature plot for neat Bioplast GS 2189 and bio-$CaCO_3$/Bioplast GS 2189 nanocomposites.

dx.doi.org/10.1021/sc400405v | ACS Sustainable Chem. Eng. 2014, 2, 706−717

Table 7. CTE Results for Neat Bioplast GS 2189 and Bio-$CaCO_3$/ Bioplast GS 2189 Nanocomposites

		CTE (μm/m °C)	
no.	sample	below T_g (40–50 °C)	above T_g (75–85 °C)
1	neat Bioplast GS 2189	142.8 ± 3.4	4203.9 ± 32.6
2	1% bio-$CaCO_3$/Bioplast GS 2189 nanocomposite	139.1 ± 1.2	3944.7 ± 52.7
3	2% bio-$CaCO_3$/Bioplast GS 2189 nanocomposite	136.3 ± 2.2	3889.5 ± 36.2
4	2% bio-$CaCO_3$/Bioplast GS 2189 nanocomposite	140.6 ± 1.3	4021.8 ± 42.4

2189 nanocomposites show better dimensional stability in the softening region between temperatures of (55–75 °C) and below about 90 °C. The CTE values acquired from the test results are presented in Table 7, and they clearly indicate the improved thermal stability of the bionanocomposites compared to the neat polymer

Flexure tests were carried out to investigate the effect of bio-$CaCO_3$ nanoparticles on the mechanical properties of the neat Bioplast GS 2189 thermoplastic polymer and bio-$CaCO_3$/ Bioplast GS2189 nanocomposites as well. Stress–strain curves of tested specimens are presented in Figure 9, and the results

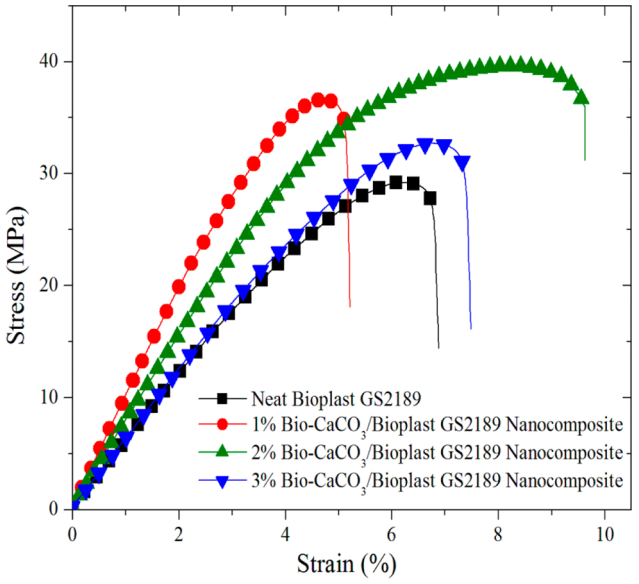

Figure 9. Stress–strain curve of flexure test for neat Bioplast GS 2189 and bio-$CaCO_3$/Bioplast GS 2189 nanocomposites.

are listed in Table 8. The flexure strength for neat Bioplast GS 2189 is 29.23 MPa, and as the bio-$CaCO_3$ nanoparticles loading increases, the flexure strength remarkably increases by 25.24% for the 1% samples, 35.3% for the 2% samples, and 11.77% for the 3% samples. A similar trend was observed for the flexural modulus. The flexure modulus for the neat Bioplast GS 2189 polymer was 5.8 MPa, whereas for the 1% bio-$CaCO_3$/Bioplast GS2189 nanocomposite, the flexure modulus increased significantly by 57.2% (9.1 MPa). Nanophased Bioplast GS2189 with loadings of 2% and 3% bio-$CaCO_3$ nanoparticles also exhibited an increase in the flexure modulus by 30.5% and 6.9%, respectively.

A common trend in nanoparticles-reinforced polymer tested in flexure configuration is the increase in strength and modulus, but on the other hand, nanofiller reinforcements may have a detrimental effect on the flexural strain to break.[51] Many researchers have reported a decrease in the failure strains of different polymers upon the addition of reinforcing fillers as the resultant composite become more brittle.[52−55] Interestingly, in this investigation, bio-$CaCO_3$/Bioplast GS2189 nanocomposites exhibited a significant increase in the strain-to-failure compared to the neat Bioplast GS2189 polymer. The strain-to-failure for the neat polymer was 3.8%, while it was 4.75% and 6.8% for 1% and 3% bio-$CaCO_3$/Bioplast GS2189 nanocomposites, respectively. The addition of bio-$CaCO_3$ nanoparticles results in a maximal increase of 8.39% of strain-to-failure at 2% loading. The bio-$CaCO_3$/Bioplast GS2189 nanocomposite sample with 2% loading was very ductile and never failed with the increase in flexure loading; however, some cracks appeared in the tested samples.

The enhancement in the mechanical properties of bio-$CaCO_3$/Bioplast GS2189 nanocomposites is due to the presence of well-dispersed highly porous bio-$CaCO_3$ nanoparticles. In addition to good bionanoparticles dispersion, some important characteristics of the as-prepared bionanocomposites have to be considered such as the quality of the interface in as-prepared bionanocomposites and the interfacial stiffness that plays an important role in the materials' capability to transfer load and stresses between matrix and the nanofillers, allowing the rigid nanoparticles to efficiently contribute in carrying the load and enhancing the mechanical properties.[56]

The morphology of the fracture surfaces of neat Bioplast GS 2189 and the bio-$CaCO_3$/Bioplast GS 2189 nanocomposite was investigated by SEM, and the fractographs are presented in Figure 10. Figure 10a shows that the fracture surface of neat Bioplast GS 2189 is relatively smooth, while it is rough and uneven for the 1% bio-$CaCO_3$/Bioplast GS 2189 nanocomposite and 3% bio-$CaCO_3$/Bioplast GS 2189 nanocomposite as illustrated in Figure 10b and c, respectively. For the 2% bio-$CaCO_3$/Bioplast GS 2189 nanocomposite sample, the fracture surface was not examined by SEM as the samples did not fail during the flexure test. Figure 11 shows optical micrographs of the sample. As shown in Figure 11a, the sample has cracked on the tensile stress zone and the crack propagated

Table 8. Flexure Test Results for Neat Bioplast GS 2189 and Bio-$CaCO_3$/Bioplast GS 2189 Nanocomposites

no.	sample	flexural strength (MPa)	increase (%)	flexural modulus (GPa)	increase (%)	strain at max strength	increase (%)
1	neat Bioplast GS 2189	29.2 ± 2.7	–	5.8 ± 1.3	–	6.3 ± 0.7	–
2	1% bio-$CaCO_3$/Bioplast GS 2189 nanocomposite	36.6 ± 1.4	25.2	9.1 ± 0.9	56.9	4.8 ± 0.5	−24.6
3	2% bio-$CaCO_3$/Bioplast GS 2189 nanocomposite	39.6 ± 1.7	35.3	7.6 ± 1.1	30.5	8.4 ± 1.0	33.3
4	3% bio-$CaCO_3$/Bioplast GS 2189 nanocomposite	32.7 ± 2.1	11.8	6.2 ± 1.5	06.9	6.8 ± 0.8	07.9

dx.doi.org/10.1021/sc400405v | ACS Sustainable Chem. Eng. 2014, 2, 706−717

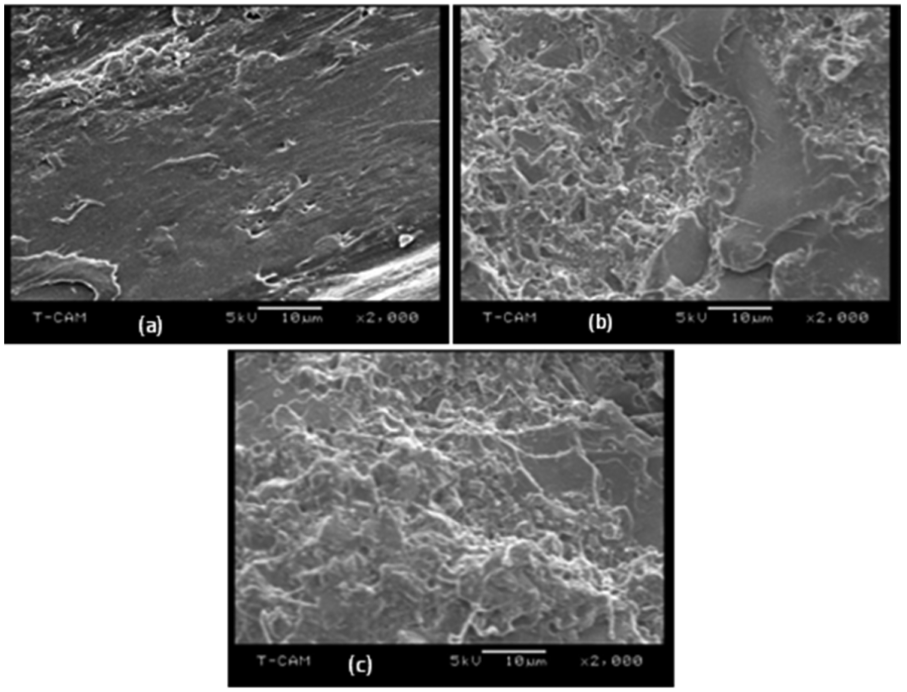

Figure 10. Fracture surfaces for (a) neat and bio-$CaCO_3$/Bioplast GS 2189 (b, c) 1% and 3% bio-$CaCO_3$/Bioplast GS 2189 nanocomposites, respectively.

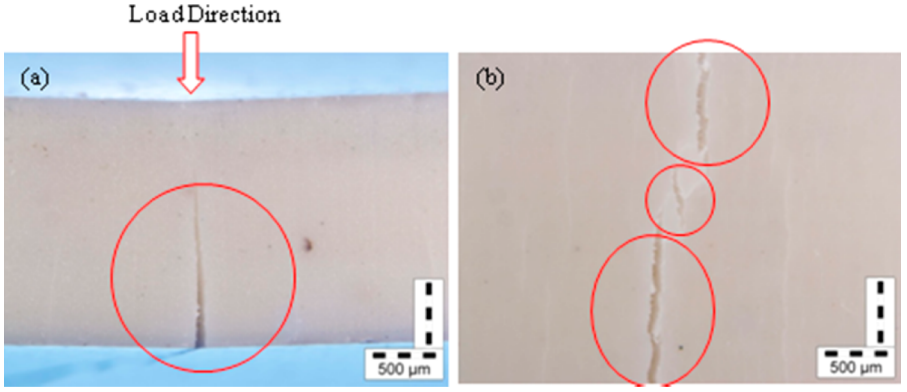

Figure 11. Optical microscope micrographs of 2% bio-$CaCO_3$/Bioplast GS 2189 nanocomposite sample.

through the sample. In Figure 11b, the lower side of the sample is shown, and it is clear from the image that increasing the load during the test has created several cracks within the tensile stress side of the sample. These images suggest that the crack growth was difficult and did not propagate to cause failure due to the enhanced mechanical properties of the sample. The fracture surface studies for neat Bioplast GS 2189 and the bio-$CaCO_3$/Bioplast GS 2189 nanocomposite are in agreement with the flexure test results.

CONCLUSIONS

This investigation has successfully demonstrated the fabrication of bionanocomposite materials derived from renewable resources with enhanced thermal and mechanical properties. Novel bionanocomposites were produced via the incorporation of bio-$CaCO_3$ nanoparticles derived from eggshells as nanofillers in Bioplast GS 2189 thermoplastic biopolymer. The bio-$CaCO_3$ nanoparticles were efficiently dispersed and highly exfoliated in the polymer matrix via the solution mixing process, which was confirmed by XRD and TEM studies. Thermal analysis results have shown that the as-fabricated bionanocomposites are thermally more stable than their pristine counterparts. The mechanical properties of as-prepared bionanocomposites have increased substantially. The 2% bio-$CaCO_3$/Bioplast GS 2189 nanocomposite exhibited a 35.3% and 30.5% increase in the flexural strength and modulus, respectively, when compared to pristine Bioplast GS 2189 polymer. Moreover, the 2% bio-$CaCO_3$/Bioplast GS 2189 nanocomposite demonstrated a significant increase by 33.3% in the strain-to-failure compared to the neat Bioplast GS 2189 polymer. The fracture surfaces investigations were in agreement with the mechanical test results.

Dynamic mechanical analysis proved that as-prepared bionanocomposites have demonstrated a considerable enhancement in the storage modulus, loss modulus, and tan δ when compared to the neat Bioplast GS 2189 polymer. Equally important, thermo-mechanical analyses showed a significant decrease in the coefficients of thermal expansion of all loadings of bio-$CaCO_3$ in Bioplast GS 2189 compared to the coefficient of thermal expansion of pristine Bioplast GS 2189 before and

dx.doi.org/10.1021/sc400405v | ACS Sustainable Chem. Eng. 2014, 2, 706−717

after the glass transition temperature. This important increase in the materials properties at low loadings of the nanofillers highlights the importance of this new class of biobased materials. The biodegradability of as-prepared bio-$CaCO_3$/Bioplast GS 2189 nanocomposites introduce a novel material for food packaging applications that demonstrate excellent properties and eliminate the environmental issues of disposal.

AUTHOR INFORMATION

Corresponding Author

*E-mail: rangariv@mytu.tuskegee.edu.

Notes

The authors declare no competing financial interest.

ACKNOWLEDGMENTS

The financial support of the NSF-CREST #1137681, Alabama EPSCoR #1158862, and The Alabama Commission on Higher Education is gratefully acknowledged.

REFERENCES

(1) Avella, M.; Buzarovska, A.; Errico, M.; Gentile, G.; Grozdanov, A. Eco-challenges of bio-based polymer composites. *Materials* **2009**, *2*, 911−925.

(2) Adeosun, S.; Lawal, G.; Balogun, S.; Akpan, E. Review of green polymer nanocomposites. *J. Miner. Mater. Charact. Eng.* **2012**, *11* (4), 385−416.

(3) Masoodi, R.; El-Hajjar, R.; Pillai, K.; Sabo, R. Mechanical characterization of a cellulose nanofiber and bio-based epoxy composite. *Mater. Des.* **2012**, *36*, 570−576.

(4) Campanella, A.; La Scala, J.; Wool, R. Fatty acid based comonomers as styrene replacements in soybean and castor oil based thermosetting polymers. *J. Appl. Polym. Sci.* **2011**, *119*, 1000−1010.

(5) Senoz, E.; Stanzione, J.; Reno, K.; Wool, R.; Miller, M. Pyrolyzed chicken feather fibers for biobased composite reinforcement. *J. Appl. Polym. Sci.* **2013**, *128* (2), 983−989.

(6) Mingjiang, Z.; Wool, R. Thermal expansivity of chicken feather fiber reinforced epoxy composites. *J. Appl. Polym. Sci.* **2013**, *128* (2), 997−1003.

(7) Lu, D.; Xiao, C.; Xu, S. Starch-based completely biodegradable polymer materials. *eXPRESS Polym. Lett.* **2009**, *3* (6), 366−375.

(8) Soares, F.; Yamashita, F.; Müller, C.; Pires, A. Thermoplastic starch/poly(lactic acid) sheets coated with cross-linked chitosan. *Polym. Test.* **2013**, *32*, 94−98.

(9) Gwon, J.; Lee, S.; Chun, S.; Doh, G.; Kim, J. Effects of chemical treatments of hybrid fillers on the physical and thermal properties of wood plastic composites. *Composites, Part A* **2010**, *41*, 1491−1497.

(10) Rosch, J.; Mulhaupt, R. Polymers from renewable resoureces: Polyester resins and blends based upon anhydride-cured epoxidized soybean oil. *Polym. Bull.* **1993**, *31*, 679−685.

(11) Erkske, D.; Viskere, I.; Dzene, A.; Tupureina, V.; Savenkova, L. Biobased polymer composites for films and coatings. *Proc. Est. Acad. Sci., Chem.* **2006**, *55* (2), 70−77.

(12) Rodriguez, C.; Medina, J.; Reinecke, H. New thermoplastic materials reinforced with cellulose based fibers. *J. Appl. Polym. Sci.* **2003**, *90* (13), 3466−3472.

(13) Wool, R.; Schiltz, D.; Steiner, D. Injection Moldable Biodegradable Starch Polymer Composites. U.S. Patent 5,162,392. 1992.

(14) Wool, R.; Kusefoglu, S.; Zhao, R.; Palmese, G.; Khot, S. High Modulus Polymers and Composites from Plant Oils. U.S. Patent 6,121,398, 2000.

(15) Wool, R.; Bunker, S. P. Pressure Sensitive Adhesives from Plant Oils. U.S. Patent 6,646,033, 2003.

(16) Wool, R.; Lu, J.; Khot, S. N. Sheet Molding Compound from Plant Oils. U.S. Patent 6,900,261, 2005.

(17) Lin, Z.; Guan, Z.; Chen, C.; Cao, L.; Wang, Y.; Gao, S.; Xu, B.; Li, W. Preparation, structures and properties of shell/polypropylene biocomposites. *Thermochim. Acta* **2013**, *551*, 149−154.

(18) Toro, P.; Quijada, R.; Arias, J.; Yazdani-Pedram, M. Mechanical and morphological studies of poly(propylene)-filled eggshell composites. *Macromol. Mater. Eng.* **2007**, *292* (9), 1027−1034.

(19) Toro, P.; Quijada, R.; Yazdani, P.; Mehrdad, A.; Arias, J. L. Eggshell, a new biofiller for polypropylene composites. *Mater. Lett.* **2007**, *61* (22), 4347−4350.

(20) Arias, J.; Quijada, R.; Toro, P.; Yazdani, P. Polypropylene Composites with Reinforcement Based on Eggshells. U.S. Patent 7,459,492 B2, 2008.

(21) Ji, G.; Zhu, H.; Qi, C.; Zeng, M. Mechanism of interactions of eggshell microparticles with epoxy resin. *Polym. Eng. Sci.* **2009**, *49* (7), 1383−1388.

(22) Kang, D.; Pal, K.; Park, S.; Bang, D.; Kim, J. Effect of eggshell and silk fibroinon styrene−ethylene/butylene−styrene as bio-filler. *Mater. Des.* **2010**, *31* (4), 2216−2219.

(23) Tsai, W.; Yang, J.; Hsu, H.; Lin, C.; Lin, K.; Chiu, C. Development and characterization of mesoporosity in eggshell ground by planetary ball Milling. *Microporous Mesoporous Mater.* **2008**, *111*, 379−386.

(24) Arias, J.; Fink, D.; Xiao, S.; Heuer, A.; Caplan, A. Biomineralization and eggshells: Cell-mediated a cellular compartments of mineralized extracellular matrix. *Int. Rev. Cytol.* **1993**, *145*, 217−250.

(25) Arias, J.; Fernandez, M. Biomimetic processes through the study of mineralized shells. *Mater. Charact.* **2003**, *50*, 189−195.

(26) Lammie, D.; Baina, M.; Wess, T. Microfocus X-ray scattering investigations of eggshell nanotexture. *J. Synchrotron Radiat.* **2005**, *12*, 721−726.

(27) Hassan, T.; Rangari, V.; Jeelani, S. Mechanical and thermal properties of bio-based $CaCO_3$/soybean-based hybrid unsaturated polyester nanocomposites. *J. Appl. Polym. Sci.* **2013**, *130*, 1442−1452.

(28) Takamine, K.; Bhatnagar, S.; Hanna, M. Effect of eggshell on properties of corn starch extrudates. *Cereal Chem.* **1995**, *72* (4), 385−388.

(29) Xu, Y.; Hanna, M. Effect of eggshell powder as nucleating agent on the structure, morphology and functional properties of normal corn starch foams. *Packag. Technol. Sci.* **2007**, *20*, 165−172.

(30) Bootklad, M.; Kaewtatip, K. Biodegradation of thermoplastic starch/eggshell powder composites. *Carbohydr. Polym.* **2013**, *97*, 315−320.

(31) Barber, B.; Putterman, S. Spectrum of synchronous picosecond sonoluminescence. *Phys. Rev. Lett.* **1992**, *69*, 1182−1184.

(32) Suslick, K. *The Mechanochemical Effects of Ultrasound*; Proc. First Intl. Conf. Mechanochemistry, Cambridge Interscience: Cambridge, 1994, vol. *1*, pp 43−49.

(33) Franco, F.; Perez-Maqueda, L.; Perez-Rodriguez, J. The influence of ultrasound on the thermal behaviour of a well ordered kaolinite. *Thermochim. Acta* **2003**, *404*, 71−79.

(34) Franco, F.; Perez-Maqueda, L.; Perez-Rodriguez, J. The effect of ultrasound on the particle size and structural disorder of a well-ordered kaolinite. *J. Colloid Interface Sci.* **2004**, *274*, 107−117.

(35) Franco, F.; Perez-Maqueda, L.; Perez-Rodriguez, L. Influence of the particle-size reduction by ultrasound treatment on the dehydroxylation process of kaolinites. *J. Therm. Anal. Calorim.* **2004**, *78*, 1043−1055.

(36) Suslick, K.; Didenko, Y.; Fang, M.; Hyeon, T.; Kolbeck, K.; McNamara, W., III; Mdleleni, M.; Wong, M. Acoustic cavitation and its chemical consequences. *Philos. Trans. R. Soc., A* **1999**, *357*, 335−353.

(37) Misik, V.; Kirschenbaum, L. J.; Riesz, P. Free radical production by sonolysis of aqueous mixtures of N,N-dimethylformamide: An EPR spin trapping study. *J. Phys. Chem.* **1995**, *99*, 5970.

(38) Vijaya Kumar, R.; Diamant, Y.; Gedanken, A. Sonochemical synthesis and characterization of nanometersize-size transition metal oxides from metal acetates. *Chem. Mater.* **2000**, *12*, 2301−2305.

(39) Hassan, T.; Rangari, V.; Rana, R.; Jeelani, S. Sonochemical effect on size reduction of $CaCO_3$ nanoparticles derived from waste eggshells. *Ultrason. Sonochem.* **2013**, *20*, 1308−1315.
(40) Rangari, V.; Hassan, T.; Mayo, Q.; Jeelani, S. Size reduction of WO_3 nanoparticles by ultrasound irradiation and its applications in structural nanocomposites. *Compos. Sci. Technol.* **2009**, *69*, 2293−2300.
(41) Cheremisinoff, N. *Polymer Mixing and Extrusion Technology*; Marcel Dekker, Inc.: New York: 1987.
(42) Lee, J.; Ashokumar, M.; Kentish, S.; Grieser, F. Effect of alcohols on the initial growth of multibubble sonoluminescence. *J. Phys. Chem. B* **2006**, *110*, 17282−17285.
(43) Jones, W.; Rangari, V.; Hassan, T.; Jeelani, S. Synthesis and characterization of (Fe_3O_4/MWCNTs)/ epoxy nanocomposites. *J. Appl. Polym. Sci.* **2010**, *116*, 2783−2792.
(44) Cheung, H. Y.; Lau, K. T.; Tao, X. M.; Hui, D. A potential material for tissue engineering: Silkworm silk/PLA Biocomposite. *Composites, Part B* **2008**, *39*, 1026−1033.
(45) Loera, A. G.; Cara, F.; Dumon, M.; Pascault, J. P. Porous epoxy thermosets obtained by a polymerization-induced phase separation process of a degradable thermoplastic polymer. *Macromolecules* **2002**, *35*, 6291−6297.
(46) Signori, F.; Coltelli, M. B.; Bronco, S. Thermal degradation of poly(lactic acid) and poly(butylenesadipate-co-terephthalate) and their blends upon melt processing. *Polym. Degrad. Stab.* **2009**, *94*, 74−82.
(47) Yang, S.; Wu, Z. H.; Yang, W.; Yang, M. B. Thermal and mechanical properties of chemical crosslinked polylactide (PLA). *Polymer Testing.* **2008**, *27*, 957−963.
(48) Ray, S.; Okamoto, K.; Okamoto, M. Structure−property relationship in biodegradable poly(butylene succinate)/layered silicate nanocomposites. *Macromolecules* **2003**, *36*, 2355−2367.
(49) Huda, M. S.; Drzal, L. T.; Mohanty, A. K.; Misra, M. Chopped glass and recycled newspaper as reinforcement fibers in injection molded poly(lactic acid) (PLA) composites: A comparative study. *Compos. Sci. Technol.* **2006**, *66*, 1813−1824.
(50) Rana, A. K.; Mitra, B. C.; Banerjee, A. N. Short jute fiber-reinforced polypropylene composites: Dynamic mechanical study. *J. Appl. Polym. Sci.* **1999**, *71* (4), 531−539.
(51) Nielsen, L.; Landel, R. *Mechanical Properties of Polymers and Composites*; Marcel Decker, Inc,.: New York. 1994.
(52) Wang, S. F.; Shen, L.; Zhang, W. D.; Tong, Y. J. Preparation and mechanical properties of chitosan/carbon nanotubes composites. *Biomacromolecules* **2005**, *6* (6), 3067−3072.
(53) Xu, C.; Jia, Z.; Wu, D.; Han, Q.; Meek, T. Fabrication of nylon-6/carbon nanotube composites. *J. Electron. Mater.* **2006**, *35* (5), 954−957.
(54) Xu, M.; Zhang, T.; Gu, B.; Wu, J.; Chen, Q. Synthesis and properties of novel polyurethane/MWCNT composites. *Macromolecules* **2006**, *39* (10), 3540−3545.
(55) Meincke, O.; Kaempfer, D.; Weickmann, H.; Friedrich, C.; Vathauer, M.; Warth, H. Mechanical properties and electrical conductivity of carbon-nanotube filled polyamide-6 and its blends with acrylonitrile/butadiene/styrene. *Polymer* **2004**, *45* (3), 739−748.
(56) Zhang, M.; Zeng, H.; Zhang, L.; Lin, G.; Li, R. Fracture characteristics of discontinuous carbon fibre-reinforced PPS and PES-C composites. *Polym. Polym. Compos.* **1993**, *1*, 357−365.